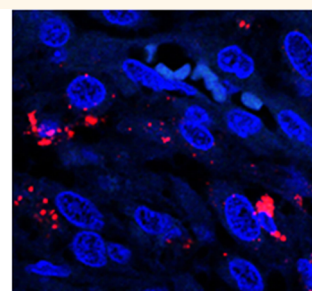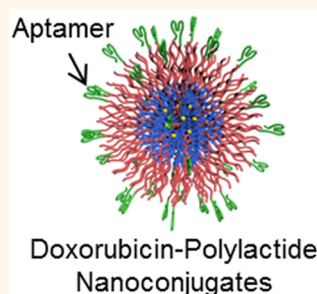# Targeting Tumor Vasculature with Aptamer-Functionalized Doxorubicin–Polylactide Nanoconjugates for Enhanced Cancer Therapy

Li Tang,[†] Rong Tong,[†] Virginia J. Coyle,[‡] Qian Yin,[†] Holly Pondenis,[‡] Luke B. Borst,[§] Jianjun Cheng,*[,†] and Timothy M. Fan*[,‡]

[†]Department of Material Sciences and Engineering and [‡]Department of Veterinary Clinical Medicine, University of Illinois at Urbana–Champaign, Urbana, Illinois 61801, United States and [§]Department of Population Health and Pathobiology, North Carolina State University, Raleigh, North Carolina 27607, United States

**ABSTRACT** An A10 aptamer (Apt)-functionalized, sub-100 nm doxorubicin–polylactide (Doxo-PLA) nanoconjugate (NC) with controlled release profile was developed as an intravenous therapeutic strategy to effectively target and cytoreduce canine hemangiosarcoma (cHSA), a naturally occurring solid tumor malignancy composed solely of tumor-associated endothelium. cHSA consists of a pure population of malignant endothelial cells expressing prostate-specific membrane antigen (PSMA) and is an ideal comparative tumor model system for evaluating the specificity and feasibility of tumor-associated endothelial cell targeting by A10 Apt-functionalized NC (A10 NC). *In vitro*, A10 NCs were selectively internalized across a panel of PSMA-expressing cancer cell lines, and when incorporating Doxo, A10 Doxo-PLA NCs exerted greater cytotoxic effects compared to nonfunctionalized Doxo-PLA NCs and free Doxo. Importantly, intravenously delivered A10 NCs selectively targeted PSMA-expressing tumor-associated endothelial cells at a cellular level in tumor-bearing mice and dramatically increased the uptake of NCs by endothelial cells within the local tumor microenvironment. By virtue of controlled drug release kinetics and selective tumor-associated endothelial cell targeting, A10 Doxo-PLA NCs possess a desirable safety profile *in vivo*, being well-tolerated following high-dose intravenous infusion in mice, as supported by the absence of any histologic organ toxicity. In cHSA-implanted mice, two consecutive intravenous infusions of A10 Doxo-PLA NCs exerted rapid and substantial cytoreductive activities within a period of 7 days, resulting in greater than 70% reduction in macroscopic tumor-associated endothelial cell burden as a consequence of enhanced cell death and necrosis.

**KEYWORDS:** nanoconjugate drug delivery · cancer targeting by aptamer · tumor-associated endothelium · comparative tumor model · prostate-specific membrane antigen

The sustained growth of solid tumors requires the development of tumor-associated neovasculature for the provision of oxygen, nutrients, and growth factors, which are necessary for cancer progression and survival.[1] Without adequate vascularization, tumor cells undergo programmed cell death and necrosis, which results in the regression of macroscopic tumor burdens. Given the indispensable nature of angiogenesis, targeting endothelial cells that constitute a major component of tumor-associated neovasculature has emerged as a complementary and potentially effective anticancer treatment strategy.[2] Tumor-associated neovasculature is qualitatively distinct from normal blood vessels, with differences in structural elements, morphologic organization, and physiologic functions,[3] and the differential expression of specific membranous epitopes by tumor-associated endothelial cells provides the opportunity to selectively target and disrupt tumor neovasculature, with consequent death of vascular-dependent cancer cells.

Prostate-specific membrane antigen (PSMA), a transmembrane protein that was originally identified to be overexpressed by malignant epithelial cells of prostatic carcinoma origin, is also expressed by endothelial cells of tumor-associated neovasculature but not by normal endothelial cells.[4,5] Given its dichotomous

©2015 American Chemical Society

expression, PSMA is an ideal target for the delivery of diagnostic probes and therapeutics directly to tumor-associated neovasculature. For prostatic carcinoma patients, several PSMA-targeting strategies for *in vivo* whole body imaging have been developed and validated and include antibodies that recognize the extracellular domain of PSMA or small molecules that bind to the PSMA enzymatic domain.[6] In addition to diagnostic imaging, antibodies that target PSMA have been incorporated into drug delivery strategies for the treatment of prostate cancer and include conjugation of anti-PSMA antibodies with radionuclides or cytotoxins.[7−10] Although technically feasible, the incorporation of antibodies as a method of targeted drug delivery has inherent limitations based upon the large size, high cost, and potential immunogenicity of antibodies, all properties that could potentially limit their pharmacological value for wide future clinical use.[11]

Single-stranded oligonucleotide ligands, termed aptamers (Apts), which fold into specific three-dimensional conformations for selective binding to target antigens with high affinity and specificity, have been recently demonstrated to rival antibodies as targeting ligands[12−15] and have proved efficacious for the management of neoplastic and non-neoplastic pathologies.[16−19] Compared with antibodies, Apts have several favorable properties as cancer-targeting ligands, which include their small size, low immunogenicity, and lower production costs. Importantly, Apts can be easily functionalized with controllable chemical functional groups on their termini to permit orthogonal conjugations.[20] Recently, synthetic single-strand RNA Apts (A9 and A10 Apts) have been identified to bind specifically and with nanomolar affinity to the extracellular domain of PSMA.[21] These Apts have been demonstrated to selectively target prostate cancer cells that express PSMA *in vitro* and *in vivo*.[14,22−25] However, these PSMA Apts have been only narrowly explored as drug delivery targeting ligands for the detection and treatment of prostate cancers specifically, and the broader applicability of PSMA Apts for targeting tumor-associated vasculature, which is indispensable for the progressive growth of all solid tumors, has yet to be investigated in sophisticated preclinical model systems.

We have recently developed doxorubicin−polylactide (Doxo-PLA) nanoconjugates (NCs) with well-controlled formulation properties for anticancer drug delivery. These Doxo-PLA NCs are sub-100 nm in size with narrow particle size distribution, have high drug loadings (up to ~30 wt %), and show sustained release of Doxo without burst liberation.[26] The controlled release of Doxo could potentially minimize dose-limiting toxicities associated with free Doxo, which includes acute nephrotoxicity and cumulative cardiotoxicity.[27,28] Further surface engineering of these NCs with cancer-targeting ligands (*e.g.*, Apts) should theoretically result in targeted and controlled drug release delivery systems with improved safety profiles and antitumor activities. Here, we report an A10 Apt-functionalized, sub-100 nm Doxo-PLA NC (A10 Doxo-PLA NC) with controllable release profile for targeting canine hemangiosarcoma (cHSA), a naturally occurring solid malignancy composed solely of primitive angiogenic malignant endothelial cells.[29] Unlike human umbilical vein endothelial cells, which must be induced to express PSMA *in vitro*[30] and do not exhibit malignant characteristics *in vivo*, cHSA cells have the capacity to rapidly grow into macroscopic and invasive tumors consisting of a pure population of malignant endothelial cells that express PSMA and therefore serve as an ideal preclinical model for assessing the tumor-associated endothelial targeting specificity of PSMA Apts. We report for the first time that A10 Apt-functionalized NCs are highly effective for targeting and delivering cytotoxic payloads directly to tumor-associated endothelial cells *in vivo*, resulting in superior normal tissue tolerability and concurrent enhancement in anticancer activities. These results show the feasibility of A10 Apt-functionalized NCs as a novel drug delivery strategy for the cytoreduction of tumor-associated endothelium, which is an indispensable and conserved druggable target shared across a multitude of solid tumor histologies.

## RESULTS

**Development of A10 Doxo-PLA NCs with Controlled Formulation Properties.** The A10 Doxo-PLA NCs were prepared in a manner similar to that reported recently.[26,31] To achieve a highly controllable formulation of Doxo-PLA NCs, Doxo-PLA polymer conjugate was first synthesized *via* using Doxo as initiator for the polymerization of lactide catalyzed by a site- and chemoselective metal catalyst, *i.e.*, (BDI-EI)ZnN(TMS)$_2$ (Figure 1A). This method allows for predetermined, high drug loading and quantitative conjugation efficiency. Upon the biodegradation of PLA and hydrolysis of the ester bond between Doxo and lactide, Doxo could be released as its original form in physiological conditions. Thus, the cytotoxicity of the anticancer drug would not be compromised. In the meantime, the degradation and release profile of Doxo could be easily tuned by controlling the molecular weight (MW) of PLA polymer during the living polymerization reaction.

We used the described procedure to prepare Doxo-PLA polymer conjugate with 10 repeating units to achieve high drug loading of Doxo (as high as 27.4 wt %). The resultant Doxo-PLA polymer conjugate was mixed with PLA-PEG-COOH and nanoprecipitated in water to form PEGylated Doxo-PLA NCs (Figure 1B). Surface PEGylation of nanoparticles is routinely employed to prolong circulation, minimize nonspecific absorption, and reduce particle aggregation *in vivo*.[32] The A10 Apt bearing an amine group was covalently
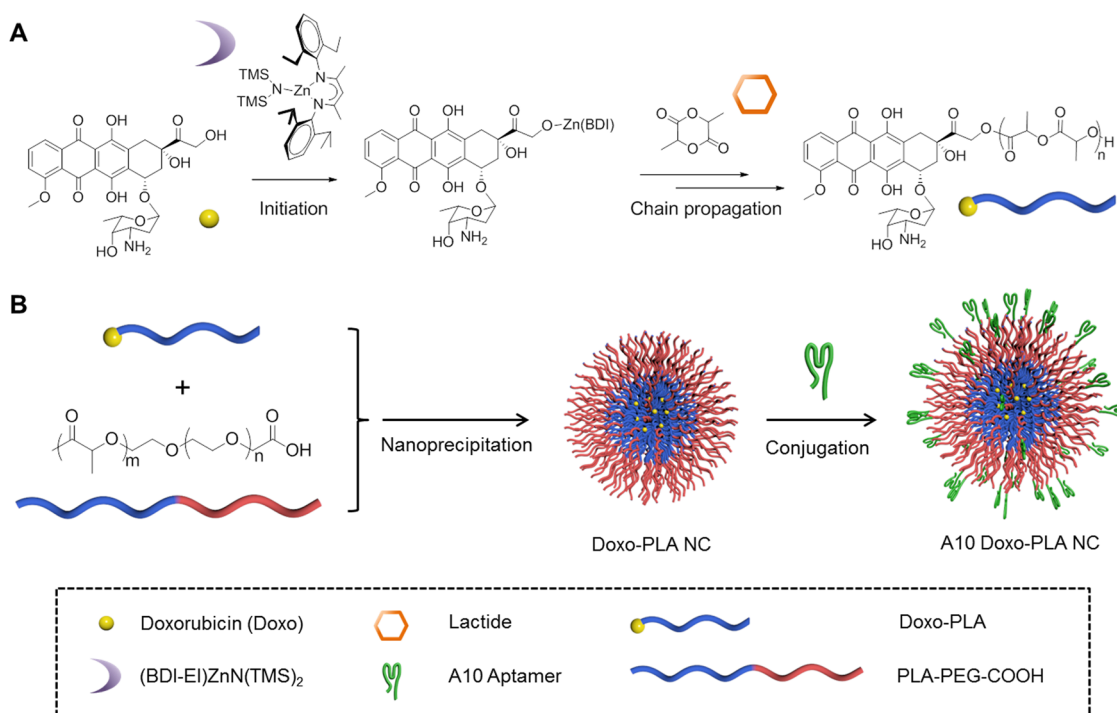
Figure 1. Preparation of A10 aptamer-functionalized doxorubicin−polylactide nanoconjugates (A10 Doxo-PLA NCs). (A) Synthesis of Doxo-PLA polymer conjugate; (B) schematic illustration of formulating A10 Doxo-PLA NCs.
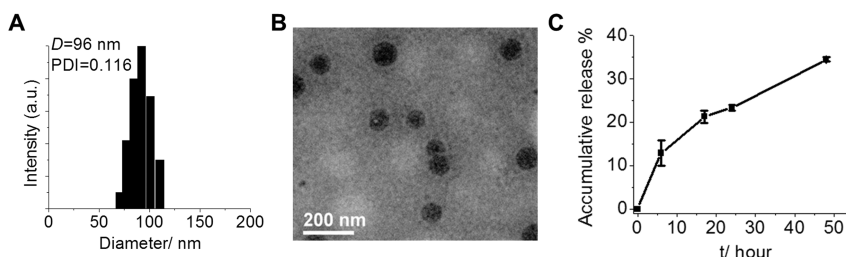


Figure 2. Characterization of A10 Doxo-PLA NCs. (A, B) Characterization of the size and size distribution of A10 Doxo-PLA NCs by DLS (A) and TEM (B). (C) Release kinetics of Doxo from A10 Doxo-PLA NCs in 50% human serum at 37 °C.

conjugated to the PEG segment with a carboxylate group through carboxylate−amine coupling reaction, forming a stable amide bond (Figure 1B). The A10 Apt conjugated to the PEG chain (MW = 5 kDa) could be extended to the solution and fully exposed due to the hydrophilicity of PEG. The resulting NCs are 96 nm in diameter with a relatively narrow particle size distribution (polydispersity = 0.116) as measured with both dynamic light scattering (DLS) and transmission electron microscopy (TEM) (Figure 2A and B). We also conducted release kinetic studies of A10 Doxo-PLA NCs in 50% (vol %) human serum to mimic the physiological conditions. These A10 Doxo-PLA NCs showed sustained release of Doxo without a burst liberation (Figure 2C).[26]

**Transcript and Protein Expressions of PSMA in cHSA Cells.** Amplicons of expected size were identified for the human and canine positive control cell lines LNCaP and CPA, respectively. No amplicons was generated for PC-3, which served as a true negative control.

Amplicons were generated for all three cHSA cell lines, confirming their expression of mRNA transcripts for PSMA (Figure 3A). Confirmation of PSMA protein expression was demonstrated by Western blot analysis (Figure 3B) and was concordant with mRNA transcript expressions. By immunohistochemistry, PSMA protein was robustly expressed by the positive control LNCaP and complete absence of staining observed in the negative control PC-3 (Figure 3C; brown, PSMA protein; blue, nucleus). Moderate positive staining for PSMA was identified in all three cHSA cell lines (Figure 3C).

*In Vitro* **Targeting of cHSA Endothelial Cells.** To evaluate the targeting capability of Apt-functionalized NCs *in vitro*, we first incubated Cy5 dye-labeled A10 NCs (A10 Cy5-PLA NCs; red, shown in Figure 3D) with control cell lines and three cHSA cell lines. The confocal imaging analysis demonstrated enhanced cellular internalization of A10 Cy5-PLA NCs in LNCaP human prostate cancer cells as well as the cHSA cell lines (SB-HSA, Cindy, and DEN). Much lower cellular uptake was
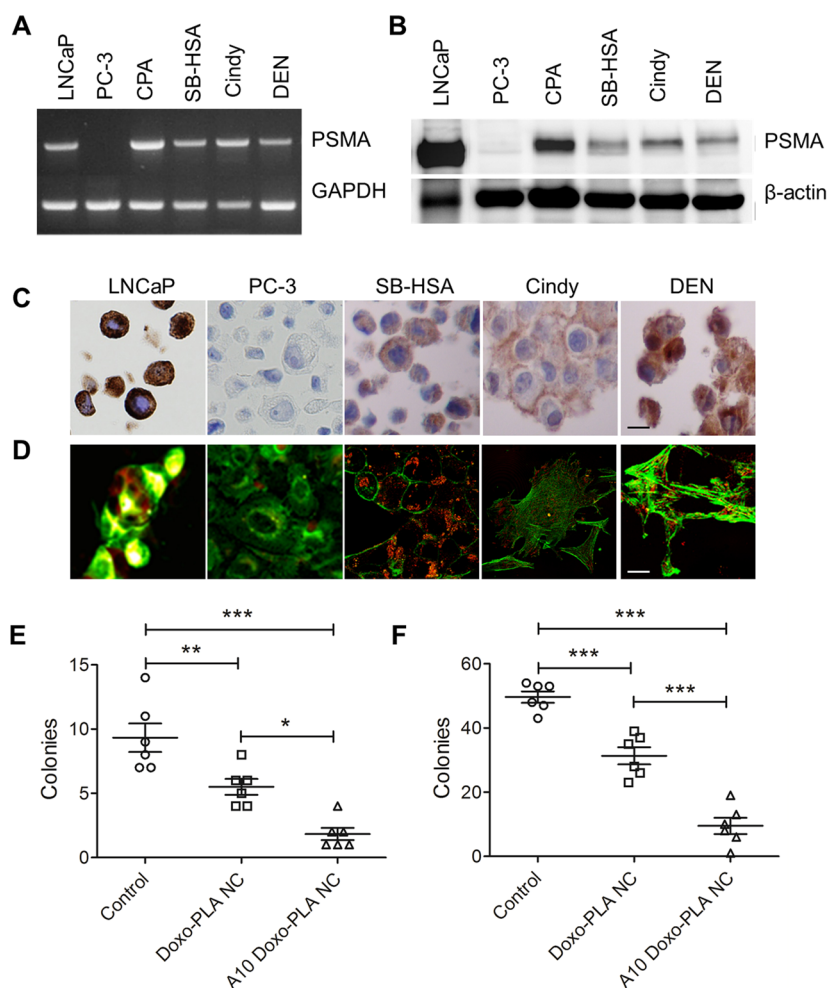
**Figure 3.** (A, B) Expressions of PSMA demonstrated by qualitative PCR (A) and Western blot analysis (B) in a panel of human and canine cell lines. (C) Detection of PSMA protein (brown) by immunohistochemistry in prostate and cHSA cell lines. Blue: nucleus. (D) Demonstration with confocal fluorescent microscopy of selective internalization of A10 Cy5-PLA NCs (red) by PSMA-expressing cell lines counterstained with phalloidin for f-actin (green). LNCaP and PC-3 serve as human PSMA positive and negative controls, respectively. CPA serves as canine PSMA positive control. Canine hemangiosarcoma cell lines: SB-HSA, Cindy, and DEN. (E, F) Ten-day colony-forming assays for two cHSA cell lines, SB-HSA (E) and Cindy (F), exposed to media only (control), nontargeting Doxo-PLA NCs, or A10 Doxo-PLA NCs following 4 h exposure duration. Greatest reduction in colony formation was achieved subsequent to A10 Doxo-PLA NCs exposure. Data are represented as average $\pm$ SEM and analyzed by one-way ANOVA and the *post hoc* Tukey test. Significance defined as *$p < 0.05$, **$p < 0.01$, ***$p < 0.001$.

observed in PC-3 cells. These observations indicate that the surface functionalization of NCs with A10 Apt results in a selective targeting effect for PSMA-expressing tumor-associated endothelial cells. To determine if enhanced cellular internalization of A10 NCs could increase *in vitro* cytotoxicity, colony-forming assays were performed with two cHSA cell lines. For SB-HSA, the number of colonies formed were 9.3 $\pm$ 1.1, 5.5 $\pm$ 0.6, and 1.8 $\pm$ 0.5 following exposure to media (control), nontargeting Doxo-PLA NCs, and A10 Doxo-PLA NCs, respectively (Figure 3E). Similar findings were observed with the Cindy cell line, with the number of colonies formed being 49.7 $\pm$ 1.8, 31.3 $\pm$ 2.7, and 9.5 $\pm$ 2.5 consequent to exposure to media (control), nontargeting Doxo-PLA NCs, and A10 Doxo-PLA NCs, respectively (Figure 3F). For both cHSA cell lines, the greatest inhibition of colony formation was achieved following

exposure to A10 Doxo-PLA NCs, which supports that the *in vitro* targeting capability of A10 Doxo-PLA NCs increases Doxo internalization and consequent cell death.

***In Vivo* Toxicity and Tissue Biodistribution of A10 NCs.** For toxicity studies, we evaluated if two desirable characteristics endowed by rationale NC fabrication strategies, being controlled drug release and PSMA-selective targeting, could dramatically reduce off-target toxicities associated with systemic Doxo administration. We intentionally utilized BALB/c mice given this strain's susceptibility to Doxo-induced focal segmental glomerulosclerosis.[33] Three weeks following a single intravenous injection of saline, free Doxo (10 mg/kg), blank A10 PLA NCs, or A10 Doxo-PLA NCs (10, 20, or 50 mg/kg Doxo equivalent), mice were sacrificed and organs were collected for histologic evaluation (Figures S1 and S2). Focal glomerulosclerosis was
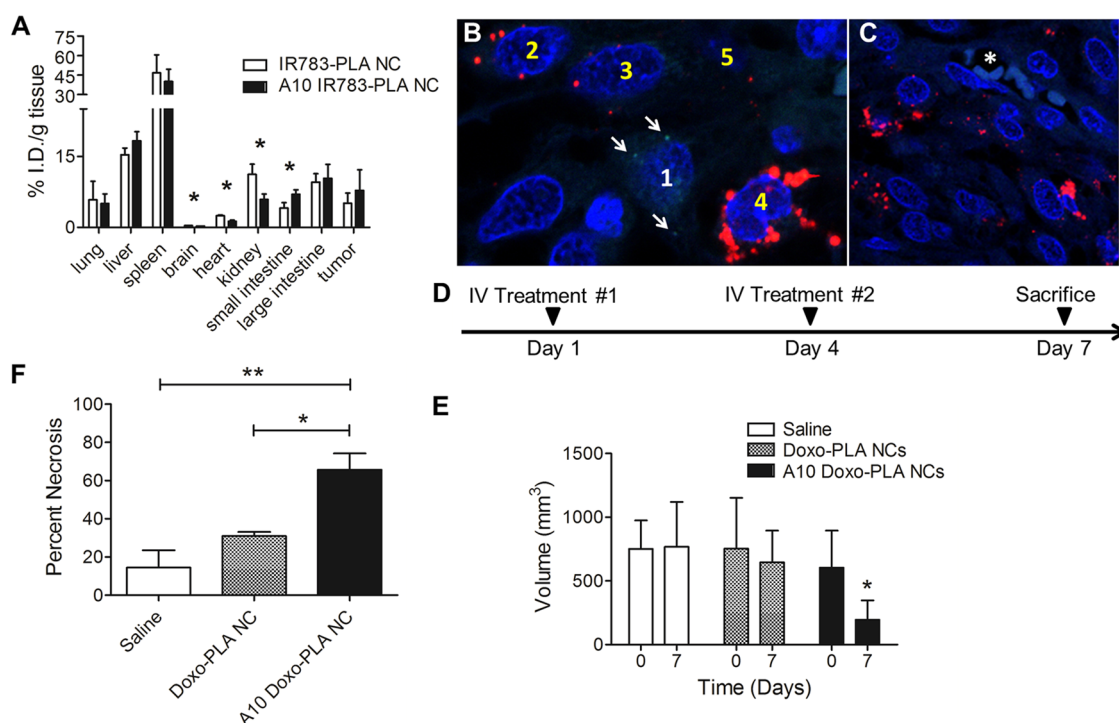
Figure 4. (A) Comparative biodistribution of A10 IR783-PLA NCs and nontargeting IR783-PLA NCs in various visceral organs and macroscopic SB-HSA tumors 24 h following intravenous administration. Data are represented as average $\pm$ SEM and analyzed by Student's $t$ test ($n = 4$). Significance defined as $*p < 0.05$. (B, C) Confocal fluorescent microscopy of PSMA-expressing SB-HSA endothelial cells growing in SCID/beige mice demonstrates highly selective subcellular internalization of A10 Cy5-PLA NCs (red), but not nontargeting Rhd-PLA NCs (green). Nuclei were stained with 4′,6-diamidino-2-phenylindole (DAPI, shown in blue). In panel B, white arrows point to small amounts of nontargeting Rhd-PLA NCs (green) within the cytoplasm of cell #1, while in contrast large quantities of internalized A10 Cy5-PLA NCs (red) can be readily identified in cells #2−5. In panel C, a panned view demonstrates abundant internalization of A10 Cy5-PLA NCs (red) by PSMA-expressing endothelial cells that make up the lumen of a blood vessel denoted by a white *. (D) In vivo treatment protocol for assessing cytoreductive activity of nontargeting and A10 Doxo-PLA NCs in SCID/beige mice growing macroscopic SB-HSA tumors. (E, F) Comparative volumetric reductions (E) and percent necrosis (F) in SB-HSA macroscopic tumors following two intravenous administrations of saline, nontargeting Doxo-PLA NCs, or A10 Doxo-PLA NCs. Data are represented as average $\pm$ SEM and analyzed by a paired $t$ test or one-way ANOVA and a post hoc Tukey test ($n = 5$). Significance defined as $*p < 0.05$, $**p < 0.01$.

identified in 3 of 4 mice treated with free Doxo (Figure S1A), while all mice treated with saline, blank A10 PLA NCs, or A10 Doxo-PLA NCs (10−50 mg/kg Doxo equivalent) were devoid of renal histologic pathology (Figure S1B−F). Additionally, no histopathologic lesions were identified in any tissues potentially affected by Doxo (heart) or expressing low levels of PSMA (brain and small intestine) following single intravenous administration of any treatments (Figure S2).

The biodistribution profiles of nontargeting NCs and A10 NCs in mice bearing macroscopic SB-HSA tumors were characterized by intravenously injecting nontargeting NCs and A10 NCs labeled with IR783, a near-infrared dye, through the lateral tail vein. Twenty-four hours postinjection, subcutaneous SB-HSA tumors and the organs were harvested and measured ex vivo for fluorescence intensity at $\lambda_{em} = 800$ nm with an Odyssey infrared imaging system (Figure S3). The accumulation of the nontargeting IR783-PLA NCs and A10 IR783-PLA NCs in the lung, liver, spleen, brain, heart, kidneys, and intestines were not markedly different. However, greater quantities of nontargeting IR783-PLA NCs accumulated in the brain, heart, and

kidney, while A10 IR783-PLA NCs deposited in the small intestine at higher concentrations (Figure 4A). For subcutaneous tumors, the total tumor accumulations of IR783-PLA NCs and A10 IR783-PLA NCs 24 h postadministration were $5.1 \pm 1.1$ and $7.8 \pm 2.2$ ID%/g (average $\pm$ SEM; $n = 4$), respectively, and were not significantly different ($p = 0.34$). To thoroughly characterize if A10 NCs could be preferentially internalized by PSMA-expressing tumor-associated endothelial cells in vivo, we further examined the suborgan distribution of nontargeting NCs and A10 NCs at the cellular level. Nontargeting NCs labeled with rhodamine (Rhd-PLA NCs, shown as green in Figure 4B with white arrows) and A10 Cy5-PLA NCs (shown as red in Figure 4B,C) were mixed and co-injected intravenously through the lateral tail vein into mice with macroscopic subcutaneous cHSA tumors. The A10-functionalized NCs showed clearly increased internalization in PSMA-expressing endothelial cells, while nontargeting NCs were primarily within the extracellular space and rarely observed in cytoplasm of the cancer cells (Figure 4B,C). These results indicate that the A10 targeting improves the internalization of the NCs by PSMA-expressing

endothelial cells *in vivo*, although the total tumor mass accumulation of NC is not dramatically different.

***In Vivo* Targeted Anticancer Activity.** The enhanced cellular uptake of A10 NCs by PSMA-expressing endothelial cells compared to nontargeting NCs suggests that Apt-functionalized NCs could potentially deliver increased amounts of cytotoxic payload to tumor-associated endothelial cells with consequent regression in tumor volume. To explore this, we evaluated the antitumor efficacy of nontargeting Doxo-PLA NCs and A10 Doxo-PLA NCs against subcutaneous macroscopic SB-HSA tumors in SCID/beige mice. After SB-HSA tumors reached 11−12 mm in diameter (600−850 mm$^3$; Figure S4), mice were equally randomized by body weight and tumor volume into three groups ($n$ = 6 per group). Mice were then treated intravenously with saline, nontargeting Doxo-PLA NCs (50 mg/kg Doxo equivalent), or A10 Doxo-PLA NCs (50 mg/kg Doxo equivalent) on days 1 and 4 (Figure 4D). Only mice that received two intravenous injections of A10 Doxo-PLA NCs showed a significant reduction in SB-HSA burden (70.6 ± 2.9% volume reduction; $p$ = 0.03, Figure S5) relative to the saline group (3.5% tumor volume increase) and nontargeting Doxo-PLA NC group (14.3 ± 8.3% volume reduction) (Figure 4E). Further histological examination of SB-HSA tissues on day 7 demonstrated that A10 Doxo-PLA NCs markedly increase the percent necrosis of PSMA-expressing endothelial tissues (65.7 ± 8.5%) compared to the SB-HSA tissues collected from mice treated with nontargeting Doxo-PLA NCs (31.0 ± 2.0%) and saline (14.5 ± 8.0%) (Figure 4F). Collectively, the *in vivo* observations support that A10 Doxo-PLA NCs exerted greater cytotoxic effects against SB-HSA tumors in mice as a consequence of enhanced cellular internalization of A10 Doxo-PLA NCs by PSMA-expressing endothelial cells in tumor.

## DISCUSSION

Due to the heterogeneity and genomic instability of individual cancer cells, resistance to conventional therapeutics commonly develops within the tumor mass and consequently results in treatment failure and progressive disease. Given the indispensable need for blood vessels to sustain the nutrient demands requisite for continued solid tumor growth, targeting the endothelium of tumor neovasculature could be highly effective in the treatment of cancers given that endothelial cells are relatively stable genetically and possess distinct druggable membrane epitopes. One such epitope is PSMA, which is a well-established and selective marker for tumor-associated endothelial cells, which form a key cellular component of solid tumor neovasculature. As such, the development of effective and safe PSMA-targeting cancer therapeutics based on Apt and NC chemistry has the potential to improve the activity of targeted cancer therapy for many types of

solid tumors and provides a low-cost, easily scalable formulation for potential therapeutic applications in cancer patients.

In this investigation, we devised a biocompatible Doxo-PLA NC platform with surface functionalization with A10 Apt for tumor-associated endothelial cell targeting. These Doxo-PLA NCs showed controlled size (sub-100 nm) and narrow particle size distribution, which in itself is favorable for passive tumor targeting through enhanced permeability and retention (EPR) effect.[34,35] The Doxo was quantitatively loaded in the NCs with high drug loadings (up to ∼30%),[26] and the simple formulation process of nanoprecipitation permits facile surface functionalization. To further improve the selective delivery of cytotoxic payloads, Doxo-PLA NCs were decorated covalently with the PSMA-specific A10 Apt, thereby allowing for the selective targeting of PSMA-expressing endothelial cells. To study the performance of the fabricated A10 NCs, we choose to use cHSA as a unique, yet powerful, translational model system. First, cHSA are derived from the hemangioblast, express genetic signatures of inflammation, and possess a primitive angiogenic endothelial phenotype, which are shared characteristics of tumor-associated endothelium.[29,36,37] Second, cHSA serves as a pure population of malignant endothelial cells that express PSMA and grow into solid tumors, dual characteristics that allow for the consistent and reproducible evaluation of PSMA-targeting drug delivery strategies both *in vitro* and *in vivo*. Last, cHSA is a naturally occurring solid malignancy that arises in pet dogs, and this natural resource of companion animals can serve as a translationally relevant comparative model for human solid tumor malignancies and evaluation of novel therapeutics that target cancer vasculature.[38]

In the present study, we demonstrated the marked increased antitumor activity of A10 Doxo-PLA NCs compared to nontargeting Doxo-PLA NCs in a cHSA preclinical tumor model. Such increased antitumor activity is likely due to the enhanced cellular internalization of A10 Doxo-PLA NCs *in vivo* rather than an absolute increase in NCs that reach the immediate tumor microenvironment. Although the biodistributions of both targeting and nontargeting NCs are essentially the same, the tissue and intracellular distributions of the differing NCs are distinct for the specific *in vivo* tumor model evaluated in this investigation. Specifically, A10 Doxo-PLA NCs are favored for intracellular uptake by PSMA-expressing endothelial cells and result in greater delivery of Doxo to the cytosol or nucleus of target cells, which leads to increased target cell death. Our observations agree well with previous reports by Kirpotin *et al.*[39] and Choi *et al.*,[40] where antibody anti-HER2 and transferrin were used as targeting ligands, respectively. It is probable that surface functionalization of NCs does not actively contribute toward homing to the tumor-associated

endothelial microenvironment, as the EPR effect dictates extravasation of NCs into the tumor mass, and is influenced by the physicochemical properties such as NC size.[40−43] However, once the NCs reach the tumor-associated microenvironment, the high affinity binding between A10 Doxo-PLA NCs and PSMA expressed on tumor-associated endothelial cells would likely promote the internalization of NCs. Thus, a significantly higher amount of A10 Doxo-PLA NCs was found within PSMA-expressing tumor endothelial cells compared to nontargeting NCs and resulted in improved antitumor activity *in vivo*. Our results support the tissue and intracellular distribution mechanism for active targeting nanomedicines and their improvement in antitumor efficacy. This mechanism may apply for different targeting ligands, *i.e.*, Apt or antibody, and different types of NPs, *i.e.*, polymeric NPs, liposomes, or gold NPs. To our knowledge, this is the first *in vivo* demonstration of incorporating A10 Apt as a highly effective targeting ligand for tumor-associated endothelial cells that results in macroscopic tumor regression. Furthermore, this strategy could also be extended to different cancer types due to the versatile overexpression of PSMA in tumor-associated neovasculature for most solid tumors, and future studies of applying this targeting strategy for other types of cancer would be essential. Importantly, the robust cytoreductive activity exerted by A10 Doxo-PLA NCs was achieved through systemic intravenous delivery rather than direct intratumoral deposition and, hence, underscores the potential for practical and clinically relevant routes of drug administration in cancer patients.

In addition to enhanced anticancer activities, our study demonstrated that the A10-functionalized NCs could reduce the dose-limiting adverse effect of Doxo. The A10 Doxo-PLA NCs were designed for controlled and sustained release of Doxo without burst release of the drug. The nephrotoxicity typically observed for free Doxo was completely avoided with A10 Doxo-PLA NCs even when 5-fold higher dosages (50 mg/kg Doxo equivalent) were given intravenously.[44,45] Free Doxo is subjected to quick renal clearance after intravenous injection due to the small size of the molecule and potentially contributes to nephrotoxicity. However, the Doxo-PLA NCs tend to accumulate in the liver and spleen, which might facilitate slower release of Doxo and consequent attenuation of acute nephrotoxicity.[46] In combination with the improved efficacy for cancer treatment, A10 Doxo-PLA NCs demonstrated highly favorable benefit-to-risk ratio in comparison with free Doxo and, hence, might serve as an alternative anthracycline-based treatment strategy for patients with existing renal or cardiac insufficiencies.

## CONCLUSIONS

In conclusion, we developed an intravenous drug delivery strategy comprised of a polylactide-based A10 Doxo-PLA NC that is surface functionalized with A10 Apt for tumor-associated endothelium targeting. These NCs showed improved cytoreductive activity against cHSA tumors in mice compared to nontargeting NCs and reduced off-target toxicity compared to free Doxo. Our findings support the tumor-targeting mechanism and associated activity might be ascribed to the enhanced cellular internalization rather than absolute increased bulk tumor accumulation, and the improved efficacy and reduced systemic toxicity of the targeting A10 Doxo-PLA NCs demonstrate their strong potential for future clinical translation.

## METHODS

**Materials.** The A10 PSMA RNA Apt ((C6-NH2) GGGAGGAc-GAuGcGGAucAGccAuGuuuAcGucAcuccuuGucAAuccucAucGGc (3′-3′dT)-5′) was synthesized by Trilink Biotechnologies (San Diego, CA, USA). Doxo·HCl was purchased from Bosche Scientific (New Brunswick, NJ, USA). D,L-Lactide (LA) was purchased from TCI America (Portland, OR, USA). All the other chemicals were purchased from Sigma-Aldrich (St. Louis, MO, USA). HPLC analyses were performed on a System Gold system (Beckman Coulter, Fullerton, CA, USA) equipped with an Luna $C_{18}$ analytical column (Phenomenex, Torrance, CA, USA) and a UV detector. The size and polydispersity of the PLA NCs were measured on a ZetaPlus dynamic light scatterer (Brookhaven Instruments, Holtsville, NY, USA). The TEM analysis was performed on a JEOL 2100 Cryo-TEM system (Tokyo, Japan). The confocal fluorescence imaging was performed with a Leica SP2 laser scanning confocal microscope (Buffalo Grove, IL, USA).

**Cell Lines.** The LNCaP and PC-3 cells were obtained from the American Type Culture Collection and served as positive and negative controls for PSMA expression, respectively.[47] The canine prostatic adenocarcinoma cell line, CPA (provided by Dr. Monique Dore, University of Montreal), served as a canine positive control for PSMA expression.[48] Three cHSA cell lines, namely, DEN[49] (provided by Dr. Douglas Thamm, Colorado State University), SB-HSA[50] (provided by Dr. Stuart Helfand, Oregon State University), and Cindy (provided by Dr. Amy MacNeill, University of Illinois), were investigated for basal PSMA expression. The LNCaP and SB-HSA cell lines were cultured in RPMI-1640, the PC-3 cell line was cultured in F-12K medium, and the remaining cHSA cell lines and CPA were cultured in DMEM. All media stocks were supplemented with 10% fetal calf serum and 1% penicillin−streptomycin, and cells were grown at 37 °C in 5% $CO_2$.

**Animals.** Mice used for toxicity studies were female BALB/c strain weighing between 18 and 20 g and were purchased from Charles River Laboratories (Willington, MA, USA). Mice used for NC biodistribution and anticancer activities were female SCID/beige weighing between 16 and 18 g and were purchased from Charles River Laboratories. All animal studies were conducted with Animal Care and Use Committee approval.

**Preparation of PLA NCs.** Doxo-PLA (Doxo/LA = 1/10, mol/mol) drug−polymer conjugate was synthesized by following the previously reported procedure (Figure 1A).[26] Briefly, in a glovebox, Doxo (5.5 mg, 0.01 mmol) was dissolved in anhydrous THF (0.5 mL). (BDI-EI)ZnN(TMS)$_2$ (18.3 mg, 0.03 mmol) was added to the Doxo solution. The mixture was stirred for 15 min at room temperature (rt). Lactic acid (14.4 mg, 0.1 mmol) in THF (0.5 mL) was added dropwise to a vigorously stirred mixture of Doxo and

(BDI-EI)ZnN(TMS)$_2$. After the polymerization was complete for overnight reaction, the drug−polymer conjugate was analyzed by HPLC to determine the incorporation efficiency and loading of Doxo. The resulting Doxo-PLA was precipitated with ethyl ether (10 mL), washed with ether and methanol/acetic acid (100/1, v/v, 10 mL) to remove BDI ligand and metal catalyst, and dried under vacuum. PLA-poly(ethylene glycol)-carboxylic acid (PLA-PEG-COOH) was synthesized similarly by using heterobifunctional PEG (HO-PEG-COOH, Laysan Bio, USA) to initiate the polymerization of lactide. Cy5-PLA (Cy5/LA = 1/100, mol/mol) and rhodamine-PLA (Rhd-PLA, Rhd/LA = 1/100, mol/mol) polymer conjugates were prepared similarly as previously reported.[26,31,48,51] IR783-PEG-PLA polymer conjugate was synthesized by conjugating amine-functionalized IR783 dye[52] with PLA-PEG-COOH.

All the NCs were prepared through a nanoprecipitation method using the corresponding polymer conjugates mixed with PLA-PEG-COOH as previously reported.[26,31,48,51] For example, Doxo-PLA NCs were readily prepared through the nanoprecipitation of Doxo-PLA polymer in the presence of PLA-PEG-COOH. Briefly, Doxo-PLA conjugate in DMF (100 $\mu$L, 10 mg/mL) and PLA-PEG-COOH in DMF (100 $\mu$L, 10 mg/mL) were mixed and added dropwise into nanopure water under vigorous stirring (4 mL). The resulting suspension was purified by ultrafiltration (15 min, 3000 rpm, Ultracel membrane with 10 000 NMWL, Millipore, Billerica, MA, USA) and then characterized for particle size by dynamic light scattering and transmission electron microscopy. Cy5 (Cy5-PLA NC), Rhd (Rhd-PLA NC), or IR783, a near-infrared dye, labeled NCs (IR783-PLA NC) were prepared similarly.

**Conjugation of Aptamer to PLA NCs.** A Doxo-PLA NC (or Cy5-PLA NC or IR783-PLA NC) solution in DNase RNase-free water (1 mg/mL, 1 mL) was incubated with an aqueous solution of 1-(3-(dimethylamino)propyl)-3-ethylcarbodimide hydrochloride (400 mM, 200 mL) and N-hydroxysuccinimide (NHS) (100 mM, 200 mL) for 15 min at rt. The resulting NHS-activated NCs were reacted with 3'-NH$_2$-modified A10 PSMA Apt (1 mg/mL in DNase/RNase-free water, 50 $\mu$L). The resulting A10 NCs were washed with water (15 mL) by ultrafiltration (5 min, 1000 g, Ultracel membrane with 10 000 NMWL, Millipore) and used directly.

**Release Kinetics of Doxo-PLA NCs.** The prepared Doxo-PLA NCs (1.0 mg/mL) were dispersed in 50% human serum at 37 °C, equally distributed to 21 vials with 1 mL of NC solution per vial, and then incubated at 37 °C. At selected time intervals, the NC solution (3 vials of each group) was mixed with an equal volume of methanol (1 mL) and centrifuged at 15k rpm for 10 min. The supernatant (1 mL) was analyzed with HPLC to quantify the released Doxo as compared to a standard curve of free Doxo (at 500 nm wavelength absorption).

**Qualitative Reverse Transcriptase Polymerase Chain Reaction.** Cell lines were grown to confluence; then adherent cells were washed twice with PBS, collected with a cell scraper, and pelleted. Total RNA was isolated with RNeasy total RNA extraction kit (Qiagen, Inc., Valencia, CA, USA), assessed for purity, and reverse transcribed to cDNA using random primers (Invitrogen Life Technologies, Carlsbad, CA, USA). The cDNA was amplified by RT-PCR using degenerate primers (forward: 5'-GATGAAGCGTTTGAAGGC-3'; reverse: 5'- GCATACTTTCTTAAAAC-3') for human and canine PSMA transcripts, and GAPDH was used as a control for the RT-PCR reaction. Generated amplicons were resolved on a 2% agarose gel with ethidium bromide. Intensity of amplicons for PSMA was normalized against GAPDH using ImageJ software.

**Protein Expression of PSMA in cHSA Cell Lines.** Cell lines were grown to confluence, collected, and either lysed for Western blot analysis or pelleted by centrifugation for immunohistochemistry. For Western blot analysis, proteins were extracted using a commercial reagent (Pierce, Rockford, IL, USA) mixed with a protease inhibitor cocktail (Thermo Scientific, Waltham, MA, USA), and concentrations quantified using a commercial kit (Pierce). Seventy-five micrograms of protein was loaded per well for all cell lines, except for LNCaP, in which 25 $\mu$g of protein was loaded. All Western blot analyses were performed through the following steps: (1) protein lysates were separated by SDS-PAGE using 10% polyacrylamide gels and transferred onto nitrocellulose membranes, with blocking at rt in 5% nonfat dry milk TBS-Tween immediately before incubation with a mouse monoclonal anti-human PSMA antibody (1:500 dilution; Abcam, Cambridge, MA, USA) in 5% nonfat dry milk TBS-Tween overnight at 4 °C; (2) after primary antibody incubation, membranes were washed and incubated for 1 h with appropriate horseradish peroxidase conjugated secondary antibodies (1:1000) in 5% nonfat dry milk TBS-Tween and developed using a standard chemiluminescence detection kit (GE HealthCare Life Sciences, Piscataway, NJ, USA). For immunohistochemistry, each pellet was resuspended in 1 mL of 10% formalin for 1 h; then cell pellets were resuspended uniformly into 1 mL of 4% melted agarose gel by vortexing and then immediately centrifuged to create an agarose-embedded cell pellet. Paraffin-embedded cell pellets were sectioned every 4 $\mu$m, placed on positively charged slides, and dried for 1 h at 60 °C. Slides were deparaffinized with three sequential xylene washes and subsequently hydrated using 100%, 95%, and 70% ethanol for 2 min each, followed by a water rinse. Slides were placed in 3% hydrogen peroxide in methanol for 15 min and then treated with citrate buffer (pH 6.0) at a temperature of 120 °C for 30 s. Slides were cooled for 2 min, then placed in SuperSensitive wash buffer. A mouse monoclonal anti-human PSMA antibody (1:500; Abcam) was incubated for 30 min at rt. Slides were rinsed with SuperSensitive wash buffer, treated with Super Enhancer for 20 min at rt, and subsequently treated with Polymer-HRP for 30 min at rt and incubated with 3,3'-diaminobenzidine at rt for 5 min. Slides were washed with SuperSensitive wash buffer and counterstained with Mayer's hematoxylin for 1 min, then dehydrated and coverslipped.

**In Vitro Cell Uptake Study.** Cell lines were grown in chamber slides for 24 h and then washed with PBS once and incubated with either 100 $\mu$L of A10 Cy5-PLA NCs (1 mg/mL) or Cy5-PLA NCs for 2 h at 37 °C. Following incubation, all cells were washed with PBS three times and fixed with 4% paraformaldehyde for 5 min. Cells were rinsed with PBS and then counterstained with Alexa-Fluor 488 Phalloidin and imaged by confocal microscopy

**Clonogenic Assay.** A clonogenic assay was performed for two cHSA cell lines, SB-HSA and Cindy, which demonstrated expression of PSMA and formed discrete colonies. Initial seed densities were either 400 or 800 cells per 3 mL of media, depending upon the proliferative rate of each cell line. In six-well plates, cells were incubated at 37 °C for 24 h to allow for adherence; then wells were washed with PBS to remove all media and exposed to various experimental conditions including media alone (control), nonfunctionalized Doxo-PLA NCs (100 ng/mL Doxo equivalent), or A10 Doxo-PLA NCs (100 ng/mL Doxo equivalent) for 4 h with gentle rocking at rt. Cells were subsequently rinsed with PBS two times to remove residual Doxo or noninternalized Doxo-PLA NCs, and then cells were allowed to grow for 10 days in fresh media. Clonogenic cell survival was determined by enumerating colony formation with crystal violet staining.

**Systemic Toxicity Profile Studies.** Ten-week-old female BALB/c mice were administered a single intravenous injection of free Doxo (10 mg/kg), blank A10 PLA NCs without Doxo, or A10 Doxo-PLA NCs (10, 20, and 50 mg/kg Doxo dose equivalents) via the lateral tail vein. Mice were monitored daily for changes in clinical behavior and sacrificed after 21 days. The heart, lungs, liver, spleen, kidney, stomach, small intestine, large intestine, and bone marrow were evaluated for histologic evidence of toxicity.

**Biodistribution Study.** Ten-week-old SCID/beige mice were injected with 5 × 10$^6$ SB-HSA cells suspended in 100 $\mu$L of Hank's balanced salt solution (HBSS) subcutaneously into the right flank. Upon the development of macroscopic tumor burden (∼12 weeks), mice were intravenously injected with 150 $\mu$L of IR783-PLA NCs (10 mg/mL) or A10 IR783-PLA NCs (10 mg/mL). Twenty-four hours later, mice were sacrificed and the biodistributions of IR783-PLA NCs or A10 IR783-PLA NCs within visceral organs including the heart, lung, kidney, liver, spleen, small intestine, large intestine, and macroscopic tumor were quantified using a LI-COR Odyssey scanner (LI-COR Bioscience, Lincoln, NE, USA).

**In Vivo Cancer Cell Targeting Study.** Ten-week-old SCID/beige mice were injected subcutaneously with 5 × 10$^6$ SB-HSA cells

suspended in 100 $\mu$L of HBSS into the right flank, allowed to develop macroscopic tumors, and subsequently co-injected intravenously with a 1:1 mixture (v/v ratio; 100 $\mu$L/100 $\mu$L) of both A10 Cy5-PLA NCs (10 mg/mL) and nontargeting Rhd-PLA NCs (10 mg/mL) of equal concentration *via* the lateral tail vein. Thirty-six hours later, mice were euthanized and perfused with 6.3 mL of chilled saline over 3 min to remove residual blood volume. Following whole body perfusion, subcutaneous SB-HSA tumors were harvested, fixed, and embedded, and subsequently 4 $\mu$m thick tissues slices were mounted onto glass slides, stained with 4′,6-diamidino-2-phenylindole (DAPI), and evaluated with confocal fluorescent microscopy.

**Efficacy Study.** Ten-week-old female SCID/beige mice were injected subcutaneously with $5 \times 10^6$ SB-HSA cells in 100 $\mu$L of HBSS into the right flank. Macroscopic tumors measuring 10−12 mm in diameter were allowed to develop over 12−16 weeks, and then mice were randomized based upon tumor volume into different treatment groups ($n = 6$). Mice were intravenously administered 200 $\mu$L of either saline, nontargeting Doxo-PLA NC (50 mg/kg Doxo equivalent), or A10 Doxo-PLA NC (50 mg/kg Doxo equivalent) on days 1 and 4 and subsequently euthanized on day 7. Initial pretreatment (day 0) and final post-treatment (day 7) tumor volumes were calculated based upon caliper measurements using the ellipsoid formula: volume = $\pi/6 \times$ length $\times$ width$^2$. Upon sacrifice, subcutaneous SB-HSA tumors were excised, fixed, and stained with hematoxylin and eosin. The relative percent necrosis within each tumor as a consequence of intravenous treatment was calculated by the following formula and ImageJ software:

$$\text{Percent necrosis} = \text{(tumor necrosis surface area} / \text{total tumor surface area)} \times 100$$

*Conflict of Interest:* The authors declare no competing financial interest.

## REFERENCES AND NOTES

1. Folkman, J. Tumor Angiogenesis: Therapeutic Implications. *N. Engl. J. Med.* **1971**, *285*, 1182–1186.
2. Kerbel, R. S.; Kamen, B. A. The Anti-Angiogenic Basis of Metronomic Chemotherapy. *Nat. Rev. Cancer* **2004**, *4*, 423–436.
3. Nagy, J. A.; Dvorak, H. F. Heterogeneity of the Tumor Vasculature: The Need for New Tumor Blood Vessel Type-Specific Targets. *Clin. Exp. Metastasis* **2012**, *29*, 657–662.
4. Chang, S. S.; O'Keefe, D. S.; Bacich, D. J.; Reuter, V. E.; Heston, W. D.; Gaudin, P. B. Prostate-Specific Membrane Antigen Is Produced in Tumor-Associated Neovasculature. *Clin. Cancer Res.* **1999**, *5*, 2674–2681.
5. Chang, S. S.; Reuter, V. E.; Heston, W. D.; Bander, N. H.; Grauer, L. S.; Gaudin, P. B. Five Different Anti-Prostate-Specific Membrane Antigen (PSMA) Antibodies Confirm Psma Expression in Tumor-Associated Neovasculature. *Cancer Res.* **1999**, *59*, 3192–3198.
6. Osborne, J. R.; Akhtar, N. H.; Vallabhajosula, S.; Anand, A.; Deh, K.; Tagawa, S. T. Prostate-Specific Membrane Antigen-Based Imaging. *Urol. Oncol.* **2013**, *31*, 144–154.
7. Milowsky, M. I.; Nanus, D. M.; Kostakoglu, L.; Vallabhajosula, S.; Goldsmith, S. J.; Bander, N. H. Phase I Trial of Yttrium-90-Labeled Anti-Prostate-Specific Membrane Antigen Monoclonal Antibody J591 for Androgen-Independent Prostate Cancer. *J. Clin. Oncol.* **2004**, *22*, 2522–2531.
8. Bander, N. H.; Milowsky, M. I.; Nanus, D. M.; Kostakoglu, L.; Vallabhajosula, S.; Goldsmith, S. J. Phase I Trial of 177lutetium-Labeled J591, a Monoclonal Antibody to Prostate-Specific Membrane Antigen, in Patients with Androgen-Independent Prostate Cancer. *J. Clin. Oncol.* **2005**, *23*, 4591–4601.
9. Henry, M. D.; Wen, S.; Silva, M. D.; Chandra, S.; Milton, M.; Worland, P. J. A Prostate-Specific Membrane Antigen-Targeted Monoclonal Antibody-Chemotherapeutic Conjugate Designed for the Treatment of Prostate Cancer. *Cancer Res.* **2004**, *64*, 7995–8001.
10. Galsky, M. D.; Eisenberger, M.; Moore-Cooper, S.; Kelly, W. K.; Slovin, S. F.; DeLaCruz, A.; Lee, Y.; Webb, I. J.; Scher, H. I. Phase I Trial of the Prostate-Specific Membrane Antigen-Directed Immunoconjugate Mln2704 in Patients with Progressive Metastatic Castration-Resistant Prostate Cancer. *J. Clin. Oncol.* **2008**, *26*, 2147–2154.
11. Sapra, P.; Shor, B. Monoclonal Antibody-Based Therapies in Cancer: Advances and Challenges. *Pharmacol. Ther.* **2013**, *138*, 452–469.
12. Jayasena, S. D. Aptamers: An Emerging Class of Molecules That Rival Antibodies in Diagnostics. *Clin. Chem.* **1999**, *45*, 1628–1650.
13. Hicke, B. J.; Stephens, A. W. Escort Aptamers: A Delivery Service for Diagnosis and Therapy. *J. Clin. Invest.* **2000**, *106*, 923–928.
14. Farokhzad, O. C.; Cheng, J.; Teply, B. A.; Sherifi, I.; Jon, S.; Kantoff, P. W.; Richie, J. P.; Langer, R. Targeted Nanoparticle-Aptamer Bioconjugates for Cancer Chemotherapy in Vivo. *Proc. Natl. Acad. Sci. U.S.A.* **2006**, *103*, 6315–6320.
15. Shangguan, D.; Li, Y.; Tang, Z.; Cao, Z. C.; Chen, H. W.; Mallikaratchy, P.; Sefah, K.; Yang, C. J.; Tan, W. Aptamers Evolved from Live Cells as Effective Molecular Probes for Cancer Study. *Proc. Natl. Acad. Sci. U.S.A.* **2006**, *103*, 11838–11843.
16. Bates, P. J.; Laber, D. A.; Miller, D. M.; Thomas, S. D.; Trent, J. O. Discovery and Development of the G-Rich Oligonucleotide As1411 as a Novel Treatment for Cancer. *Exp. Mol. Pathol.* **2009**, *86*, 151–164.
17. Mongelard, F.; Bouvet, P. As-1411, a Guanosine-Rich Oligonucleotide Aptamer Targeting Nucleolin for the Potential Treatment of Cancer, Including Acute Myeloid Leukemia. *Curr. Opin. Mol. Ther.* **2010**, *12*, 107–114.
18. Zhong, Y.; Meng, F.; Deng, C.; Zhong, Z. Ligand-Directed Active Tumor-Targeting Polymeric Nanoparticles for Cancer Chemotherapy. *Biomacromolecules* **2014**, *15*, 1955–1969.
19. Gragoudas, E. S.; Adamis, A. P.; Cunningham, E. T., Jr.; Feinsod, M.; Guyer, D. R. Pegaptanib for Neovascular Age-Related Macular Degeneration. *N. Engl. J. Med.* **2004**, *351*, 2805–2816.
20. Barbas, A. S.; Mi, J.; Clary, B. M.; White, R. R. Aptamer Applications for Targeted Cancer Therapy. *Future Oncol.* **2010**, *6*, 1117–1126.
21. Lupold, S. E.; Hicke, B. J.; Lin, Y.; Coffey, D. S. Identification and Characterization of Nuclease-Stabilized RNA Molecules That Bind Human Prostate Cancer Cells *via* the Prostate-Specific Membrane Antigen. *Cancer Res.* **2002**, *62*, 4029–4033.
22. Cheng, J.; Teply, B. A.; Sherifi, I.; Sung, J.; Luther, G.; Gu, F. X.; Levy-Nissenbaum, E.; Radovic-Moreno, A. F.; Langer, R.; Farokhzad, O. C. Formulation of Functionalized PLGA-PEG Nanoparticles for in Vivo Targeted Drug Delivery. *Biomaterials* **2007**, *28*, 869–876.
23. Dhar, S.; Kolishetti, N.; Lippard, S. J.; Farokhzad, O. C. Targeted Delivery of a Cisplatin Prodrug for Safer and More Effective Prostate Cancer Therapy in Vivo. *Proc. Natl. Acad. Sci. U.S.A.* **2011**, *108*, 1850–1855.
24. Ni, X.; Zhang, Y.; Ribas, J.; Chowdhury, W. H.; Castanares, M.; Zhang, Z.; Laiho, M.; DeWeese, T. L.; Lupold, S. E. Prostate-Targeted Radiosensitization *via* Aptamer-Shrna Chimeras in Human Tumor Xenografts. *J. Clin. Invest.* **2011**, *121*, 2383–2390.
25. Yang, J.; Xie, S. X.; Huang, Y.; Ling, M.; Liu, J.; Ran, Y.; Wang, Y.; Thrasher, J. B.; Berkland, C.; Li, B. Prostate-Targeted

Biodegradable Nanoparticles Loaded with Androgen Receptor Silencing Constructs Eradicate Xenograft Tumors in Mice. *Nanomedicine* **2012**, *7*, 1297–1309.

26. Tong, R.; Cheng, J. Ring-Opening Polymerization-Mediated Controlled Formulation of Polylactide-Drug Nanoparticles. *J. Am. Chem. Soc.* **2009**, *131*, 4744–4754.

27. Unverferth, D. V.; Magorien, R. D.; Leier, C. V.; Balcerzak, S. P. Doxorubicin Cardiotoxicity. *Cancer Treat. Rev.* **1982**, *9*, 149–164.

28. van Hoesel, Q. G.; Steerenberg, P. A.; Crommelin, D. J.; van Dijk, A.; van Oort, W.; Klein, S.; Douze, J. M.; de Wildt, D. J.; Hillen, F. C. Reduced Cardiotoxicity and Nephrotoxicity with Preservation of Antitumor Activity of Doxorubicin Entrapped in Stable Liposomes in the Lou/M Wsl Rat. *Cancer Res.* **1984**, *44*, 3698–3705.

29. Fosmire, S. P.; Dickerson, E. B.; Scott, A. M.; Bianco, S. R.; Pettengill, M. J.; Meylemans, H.; Padilla, M.; Frazer-Abel, A. A.; Akhtar, N.; Getzy, D. M.; *et al.* Canine Malignant Hemangiosarcoma as a Model of Primitive Angiogenic Endothelium. *Lab. Invest.* **2004**, *84*, 562–572.

30. Liu, T.; Jabbes, M.; Nedrow-Byers, J. R.; Wu, L. Y.; Bryan, J. N.; Berkman, C. E. Detection of Prostate-Specific Membrane Antigen on HUVECs in Response to Breast Tumor-Conditioned Medium. *Int. J. Oncol.* **2011**, *38*, 1349–1355.

31. Chaney, E. J.; Tang, L.; Tong, R.; Cheng, J.; Boppart, S. A. Lymphatic Biodistribution of Polylactide Nanoparticles. *Mol. Imaging* **2010**, *9*, 153–162.

32. Caliceti, P.; Veronese, F. M. Pharmacokinetic and Biodistribution Properties of Poly(Ethylene Glycol)-Protein Conjugates. *Adv. Drug Delivery Rev.* **2003**, *55*, 1261–1277.

33. Chen, A.; Sheu, L. F.; Ho, Y. S.; Lin, Y. F.; Chou, W. Y.; Chou, T. C.; Lee, W. H. Experimental Focal Segmental Glomerulosclerosis in Mice. *Nephron* **1998**, *78*, 440–452.

34. Maeda, H.; Wu, J.; Sawa, T.; Matsumura, Y.; Hori, K. Tumor Vascular Permeability and the EPR Effect in Macromolecular Therapeutics: A Review. *J. Controlled Release* **2000**, *65*, 271–284.

35. Hobbs, S. K.; Monsky, W. L.; Yuan, F.; Roberts, W. G.; Griffith, L.; Torchilin, V. P.; Jain, R. K. Regulation of Transport Pathways in Tumor Vessels: Role of Tumor Type and Microenvironment. *Proc. Natl. Acad. Sci. U.S.A.* **1998**, *95*, 4607–4612.

36. Lamerato-Kozicki, A. R.; Helm, K. M.; Jubala, C. M.; Cutter, G. C.; Modiano, J. F. Canine Hemangiosarcoma Originates from Hematopoietic Precursors with Potential for Endothelial Differentiation. *Exp. Hematol.* **2006**, *34*, 870–878.

37. Tamburini, B. A.; Phang, T. L.; Fosmire, S. P.; Scott, M. C.; Trapp, S. C.; Duckett, M. M.; Robinson, S. R.; Slansky, J. E.; Sharkey, L. C.; Cutter, G. R.; *et al.* Gene Expression Profiling Identifies Inflammation and Angiogenesis as Distinguishing Features of Canine Hemangiosarcoma. *BMC Cancer* **2010**, *10*, 619.

38. Paoloni, M. C.; Tandle, A.; Mazcko, C.; Hanna, E.; Kachala, S.; Leblanc, A.; Newman, S.; Vail, D.; Henry, C.; Thamm, D.; *et al.* Launching a Novel Preclinical Infrastructure: Comparative Oncology Trials Consortium Directed Therapeutic Targeting of Tnfalpha to Cancer Vasculature. *PLoS One* **2009**, *4*, e4972.

39. Kirpotin, D. B.; Drummond, D. C.; Shao, Y.; Shalaby, M. R.; Hong, K.; Nielsen, U. B.; Marks, J. D.; Benz, C. C.; Park, J. W. Antibody Targeting of Long-Circulating Lipidic Nanoparticles Does Not Increase Tumor Localization but Does Increase Internalization in Animal Models. *Cancer Res.* **2006**, *66*, 6732–6740.

40. Choi, C. H.; Alabi, C. A.; Webster, P.; Davis, M. E. Mechanism of Active Targeting in Solid Tumors with Transferrin-Containing Gold Nanoparticles. *Proc. Natl. Acad. Sci. U.S.A.* **2010**, *107*, 1235–1240.

41. Tang, L.; Fan, T. M.; Borst, L. B.; Cheng, J. Synthesis and Biological Response of Size-Specific, Monodisperse Drug-Silica Nanoconjugates. *ACS Nano* **2012**, *6*, 3954–3966.

42. Tang, L.; Gabrielson, N. P.; Uckun, F. M.; Fan, T. M.; Cheng, J. Size-Dependent Tumor Penetration and in Vivo Efficacy of Monodisperse Drug-Silica Nanoconjugates. *Mol. Pharmaceutics* **2013**, *10*, 883–892.

43. Tang, L.; Yang, X.; Dobrucki, L. W.; Chaudhury, I.; Yin, Q.; Yao, C.; Lezmi, S.; Helferich, W. G.; Fan, T. M.; Cheng, J. Aptamer-Functionalized, Ultra-Small, Monodisperse Silica Nanoconjugates for Targeted Dual-Modal Imaging of Lymph Nodes with Metastatic Tumors. *Angew. Chem., Int. Ed.* **2012**, *51*, 12721–12726.

44. Injac, R.; Boskovic, M.; Perse, M.; Koprivec-Furlan, E.; Cerar, A.; Djordjevic, A.; Strukelj, B. Acute Doxorubicin Nephrotoxicity in Rats with Malignant Neoplasm Can Be Successfully Treated with Fullerenol $C_{60}(OH)_{24}$ *via* Suppression of Oxidative Stress. *Pharmacol. Rep.* **2008**, *60*, 742–749.

45. Abo-Salem, O. M. The Protective Effect of Aminoguanidine on Doxorubicin-Induced Nephropathy in Rats. *J. Biochem. Mol. Toxicol.* **2012**, *26*, 1–9.

46. Meng, H.; Xue, M.; Xia, T.; Ji, Z.; Tarn, D. Y.; Zink, J. I.; Nel, A. E. Use of Size and a Copolymer Design Feature to Improve the Biodistribution and the Enhanced Permeability and Retention Effect of Doxorubicin-Loaded Mesoporous Silica Nanoparticles in a Murine Xenograft Tumor Model. *ACS Nano* **2011**, *5*, 4131–4144.

47. Israeli, R. S.; Powell, C. T.; Corr, J. G.; Fair, W. R.; Heston, W. D. Expression of the Prostate-Specific Membrane Antigen. *Cancer Res.* **1994**, *54*, 1807–1811.

48. Tong, R.; Coyle, V. J.; Tang, L.; Barger, A. M.; Fan, T. M.; Cheng, J. Polylactide Nanoparticles Containing Stably Incorporated Cyanine Dyes for *in Vitro* and in *Vivo* Imaging Applications. *Microsc. Res. Technol.* **2010**, *73*, 901–909.

49. Thamm, D. H.; Dickerson, E. B.; Akhtar, N.; Lewis, R.; Auerbach, R.; Helfand, S. C.; MacEwen, E. G. Biological and Molecular Characterization of a Canine Hemangiosarcoma-Derived Cell Line. *Res. Vet. Sci.* **2006**, *81*, 76–86.

50. Akhtar, N.; Padilla, M. L.; Dickerson, E. B.; Steinberg, H.; Breen, M.; Auerbach, R.; Helfand, S. C. Interleukin-12 Inhibits Tumor Growth in a Novel Angiogenesis Canine Hemangiosarcoma Xenograft Model. *Neoplasia* **2004**, *6*, 106–116.

51. Tong, R.; Yala, L.; Fan, T. M.; Cheng, J. The Formulation of Aptamer-Coated Paclitaxel-Polylactide Nanoconjugates and Their Targeting to Cancer Cells. *Biomaterials* **2010**, *31*, 3043–3053.

52. Lee, H.; Berezin, M. Y.; Guo, K.; Kao, J.; Achilefu, S. Near-Infrared Fluorescent pH-Sensitive Probes *via* Unexpected Barbituric Acid Mediated Synthesis. *Org. Lett.* **2009**, *11*, 29–32.